Control Design for Robust Performance of a Direct-drive Robot

Dragan Kostić,[1] *Student Member, IEEE*, Bram de Jager,[2] and Maarten Steinbuch,[3] *Senior Member, IEEE*
Dynamics and Control Technology Group, Department of Mechanical Engineering,
Eindhoven University of Technology (TU/e), P.O. Box 513, 5600 MB Eindhoven, The Netherlands
Phone: +31 40 247 5730, Fax: +31 40 246 1418
[1]D.Kostic@tue.nl, [2]A.G.de.Jager@wfw.wtb.tue.nl, and [3]M.Steinbuch@tue.nl

***Abstract*—An experimental approach to achieve robust performance of direct-drive robot motion control is presented in this paper. It consists of: (*i*) decoupling the robot dynamics via feedback linearisation; (*ii*) frequency domain identification of the decoupled dynamics; (*iii*) compensation of these decoupled dynamics using feedback controllers designed via μ-synthesis. The designed controllers ensure robust performance, i.e., guaranteed accuracy of robot motions despite uncertainty in its dynamics and disturbances affecting the robot operation. Theoretical aspects of the control design are formulated. Its practical implementation on a direct-drive robotic arm is demonstrated in detail. Experimental investigation confirms the quality of the design: specifications on performance and robustness are practically realized.**

***Index Terms*—Robotics, Application, Disturbance modeling, Robust control, μ-synthesis.**

I. INTRODUCTION

Maintaining a desired performance of robot motion control in the presence of uncertainties in robot dynamics and disturbances is a problem that has been attracting many researchers in the recent years. Robust control strategies are introduced to stabilize robot motions when confronted with uncertainty and disturbance conditions. Together with stabilization, more advanced robust strategies should ensure performance that is robust against uncertainties and disturbances.

There are two kinds of uncertainties. The first ones are parametric, and they arise if physical values of robot inertial and/or friction parameters are not known exactly. The second ones are unmodelled dynamic effects, e.g. flexibilities. Such effects are neglected during modeling, although they might be encountered in the real physical system. As examples of disturbances, one may think of a cogging force and quantization noise. The former one is common to direct-drive robots, while the latter one arises if incremental encoders are used as position sensors.

A survey of advanced robot control methods is available in [1]. Control methods, such as adaptive and sliding-mode control can improve system performance in the presence of uncertainty and disturbance conditions. The non-linearity of these methods, however, does not facilitate a quantitative prediction of system performance for a given robustness level. This is a limiting factor for their widespread application in practice, where it is often very important to know in advance a worst-case motion accuracy for a given bandwidth of reference trajectories.

Stability robustness, disturbance rejection, and controlled transient response can be jointly and directly imposed using feedback schemes based on H_∞ control theory [2,3]. These schemes enable quantitative prediction of motion performance, given bounds on modeling uncertainty and disturbances. Moreover, for available knowledge on the system dynamics, parasitic effects, and disturbances, motion performance can be optimized. These are the reasons that make H_∞ feedback controllers appealing solutions for practical problems and motivate their application in robotics.

In this paper we show how a functional *combination* of nonlinear control and μ-synthesis can realize robust robot performance of high quality. We suggest control design in three steps: (*i*) dynamic compensation of nonlinear couplings between the robot joints via feedback linearisation [4], (*ii*) frequency-domain identification of remaining (flexible) dynamics, (*iii*) design of feedback controllers using μ-synthesis for the remaining dynamics to meet performance and robustness specifications. These three design steps are not particularly novel as long as robust control of linear motion systems is concerned. However, to the best of our knowledge they are not common in robust robot control. Especially, identification of the dynamics that remains after feedback linearisation and the feedback design dedicated to these identified dynamics are hardly encountered in the literature on robust robot control. Usually, feedback design in robotics assumes simplified plant models. High-order dynamics (flexibilities) are regarded as disturbances. In our opinion, such reasoning is conservative, as closer knowledge of the uncompensated dynamics facilitates design of appropriate compensation.

Theoretical aspects of the control design will be formulated for the general case of a robotic manipulator with *n* degrees of freedom. Practical demonstration of the design will be done for a direct-drive robot with three rotational degrees of freedom, implemented as waist, shoulder, and elbow. As similar kinematic structure is often met in industry, results obtained for the case study should be relevant for industrial cases. This paper is an extension of our previous result [5], where feedback is designed via loop-shaping and H_∞ optimization. Here we formulate a systematic control design that preserves advantages of [5] and leads to robust robot performance.

The paper is organized as follows. In the next section we will formulate the control design. Section III will describe a direct-drive robotic arm used for experimental testing. Practical control design for this robot will be explained in Section IV. Experimental assessments of the design will be done in Section V. Conclusions will be given at the end.

II. CONTROL DESIGN FOR ROBUST PERFORMANCE

Let us represent the rigid-body dynamics of a robot manipulator with *n* joints using Euler-Lagrange's equations of motion [6]:

0-7803-7729-X/03/$17.00 ©2003 IEEE.

$$\mathbf{M}(\mathbf{q}(t))\ddot{\mathbf{q}}(t)+\mathbf{h}(\mathbf{q}(t),\dot{\mathbf{q}}(t))=\boldsymbol{\tau}(t), \quad (1)$$

where $\boldsymbol{\tau}$ is the (n×1) vector of joint torques, $\mathbf{M}$ is the (n×n) inertia matrix, $\mathbf{q}$, $\dot{\mathbf{q}}$ and $\ddot{\mathbf{q}}$ are the (n×1) vectors of joint motions, speeds and accelerations, respectively, and $\mathbf{h}$ is the (n×1) vector of Coriolis/centripetal, gravity and friction effects. Steering the joint motions along the reference trajectory $\mathbf{q}_r(t)$ is the objective of the motion control problem. It can be solved using the model (1) as follows:

$$\mathbf{M}(\mathbf{q}(t))\mathbf{u}(t)+\mathbf{h}(\mathbf{q}(t),\dot{\mathbf{q}}(t))=\boldsymbol{\tau}_c(t), \quad (2)$$

where $\boldsymbol{\tau}_c$ denotes the total control law and $\mathbf{u}$ is the feedback control action. The control (2) realizes feedback linearisation of the robot dynamics and reduces the motion control problem to the linear case:

$$\ddot{\mathbf{q}}(t)=\mathbf{u}(t). \quad (3)$$

As we have already discussed in [5], the reduced control problem (3) is valid only if the law (2) perfectly matches the real robot dynamics. In practice, this rarely happens, as no robot is perfect in its implementation and, hence, the rigid-body model used in (2) is hardly an accurate description of the real robot dynamics. Instead of (3), we should rather consider control of a more general control plant $\mathbf{P}$, defined in the frequency domain:

$$\mathbf{q}(s)=\mathbf{P}(s)\mathbf{u},\ \mathbf{P}(s)=\begin{bmatrix} P_{1,1}(s) & \cdots & P_{1,n}(s) \\ \vdots & \ddots & \vdots \\ P_{n,1}(s) & \cdots & P_{n,n}(s) \end{bmatrix}. \quad (4)$$

The transfer functions on the main diagonal of $\mathbf{P}$ represent dynamics between the feedback control action at each robot joint and the angular displacement of that joint. The cross-terms represent remaining couplings between the joints after imperfect compensation of the real robot dynamics. If any of these cross-terms is not negligible, when compared with the transfer functions on the main diagonal, we can conclude that the dynamic model employed in the feedback linearisation is not sufficiently accurate. The inclusion of the cross-terms does not principally limit the design procedure, although it makes it more involved. In this paper, for the sake of clarity, we assume a situation: the plant $\mathbf{P}$ has just a diagonal structure. This implies total decoupling of the robot dynamics via (2) and simplification of the feedback control design to n single-input, single-output cases. When dealing with practical problems, the condition of total dynamic decoupling (diagonal $\mathbf{P}$) must be verified before proceeding to the feedback control design.

Each feedback design is focused on a particular transfer function $P_{i,j}(s)$ ($i=1,\ldots,n$), representing a plant to be controlled. To abbreviate notation, the indices in the subscript will be replaced with a singe one. Thus, the plant for the i-th joint will be denoted with $P_i(s)$. It is not a mere double integrator, as by virtue of (3) one would expect, but a higher order dynamical system with resonance and anti-resonance frequencies that emerge because of flexibility. Dynamics of the plant also changes for various operating conditions, as resonance frequencies and their relative damping vary with robot configuration. A plant perturbation model can represent uncertainty in the dynamics:

$$P_i^{o}(s)\rightarrow P_i^{o}(s)(1+\Delta_i(s)). \quad (5)$$

Here, $P_i^{o}(s)$ is the nominal model of the plant, and $\Delta_i(s)$ is the multiplicative uncertainty model representing difference between P_i^{o} and the real plant dynamics. The uncertainty model can be expanded as follows:

$$\Delta_i(s)=W_i^{\delta}(s)\delta_i(s). \quad (6)$$

The stable parametric weighting function W_i^{δ} should satisfy:

$$\left|W_i^{\delta}(j\omega)\right|\geq\left|\Delta_i(j\omega)\right|,\ \forall\omega\in\mathbb{R}^{+}, \quad (7)$$

to have the normalized uncertainty $\left|\delta_i(j\omega)\right|\leq 1$, $\forall\omega\in\mathbb{R}^{+}$. Here, ω denotes angular frequency defined on the continuous domain of nonnegative real numbers $\mathbb{R}^{+}=\{x\mid x\geq 0\}$.

The nominal model of the i-th plant can be determined by a spectrum analysis technique. Measurements should be done under closed-loop conditions, since the plant might not be asymptotically stable. Several frequency response functions (FRF) $G_i^k(j\omega)$ are measured for the i-th joint, assuming feedback control action u_i (i-th element of $\mathbf{u}$) as the input variable and the joint displacement q_i as the output. Denote the total number of measurements with N_i, i.e., $k=1,\ldots,N_i$. Each $G_i^k(j\omega)$ is measured while the i-th joint is moving with a low constant speed $\dot{q}_{r,i}$, while the remaining joints take some static posture, different for every k. A low constant speed is preferable to reduce the influence of friction effects on the quality of identification. This motion is performed within the joint range. A full revolution is made if the range is not limited. The direction of movement is changed after reaching the joint limit or after the full revolution. Denote with $\mathbf{q}_r^k(t)$ an (n×1) vector of set-points, used when identifying $G_i^k(j\omega)$. Elements of $\mathbf{q}_r^k(t)$ should satisfy: $\dot{q}_{r,i}^k(t)=\dot{q}_{r,i}$, and $\dot{q}_{r,j}^k(t)\equiv 0$ if $i\neq j$. There is no formal clue how to choose N_i, but, by rule of thumb, for a given joint one should adopt distant postures in the remaining joints, such as to span their ranges of motion. The specified set-points and the frequency response measurement can be achieved by applying the control law (2) with:

$$\mathbf{q}_r=\mathbf{q}_r^k,\quad \mathbf{u}:=\mathbf{K}_p(\mathbf{q}_r-\mathbf{q})+\mathbf{K}_d(\dot{\mathbf{q}}_r-\dot{\mathbf{q}})+\mathbf{n}, \quad (8)$$

where $\mathbf{K}_p=diag[k_{p,1},\ldots,k_{p,n}]$, $\mathbf{K}_d=diag[k_{d,1},\ldots,k_{d,n}]$ are matrices of positive position and velocity gains, respectively, and the (n×1) vector $\mathbf{n}$ contains a random excitation as i-th element and zeros elsewhere. Identification is more reliable if the influence of noise (e.g., quantization noise) that corrupts the measured motion coordinates is reduced. To reduce influence of the noise, $\mathbf{M}$ and $\mathbf{h}$ in (2) are computed along the reference joint motions and speeds. The reliability of identification can be enhanced if the i-th element of $\mathbf{n}$ is taken as the input variable, instead of the feedback u_i. Then, the sen-

sitivity FRF $S_i^k(j\omega) = (1 + (j\omega k_{d,i} + k_{p,i}) G_i^k(j\omega))^{-1}$ is measured first, and the plant's FRF is determined by $G_i^k(j\omega) = (1/S_i^k(j\omega) - 1)/(j\omega k_{d,i} + k_{p,i})$. Due to measurements in closed-loop, reliable results for the plant's FRF are only obtained beyond the bandwidth of the closed-loop system. A low bandwidth is thus preferable.

Once a set of frequency response measurements $\Gamma_i = \{G_i^1(j\omega), \ldots, G_i^{N_i}(j\omega)\}$ has been collected, the nominal FRF $G_i^0(j\omega)$ can be found. We have at least two possibilities:

$$G_i^0(j\omega) = \arg \min_{G_i(j\omega)} \max_k \left| \frac{G_i^k(j\omega) - G_i(j\omega)}{G_i(j\omega)} \right|, \text{ or,} \quad (9a)$$

$$G_i^0(j\omega) = \frac{1}{N_i} \sum_{k=1}^{N_i} G_i^k(j\omega). \quad (9b)$$

For each ω, the solution (9a) minimizes the distance in the complex plain between the nominal response and all the members of the set Γ_i. The solution (9b) is an average of all measured FRF's. A choice between the solutions (9a) and (9b) can be case dependent. Our experience favors the latter one, as it usually gives smoother magnitude and phase frequency response plots. Feedback design using the μ-synthesis requires a parametric description of the nominal plant model. It can be calculated by various techniques of fitting the parametric transfer function $P_i^0(j\omega)$ into the nominal frequency response data $G_i^0(j\omega)$. Our choice is a least-square fit using an output error model structure [7]. The fit may capture effects peculiar to the plant, e.g. phase lag caused by time-delay.

The next step is to construct a parametric weighting function W_i^δ that characterizes a level of uncertainty between the nominal model and the real dynamics. For that purpose, we can calculate frequency domain data that bound the uncertainty in the plant dynamics:

$$|\Delta_i(j\omega)| = \max_k \left| \frac{G_i^k(j\omega) - P_i^0(j\omega)}{P_i^0(j\omega)} \right|, \ \forall \omega \in \mathbb{R}^+. \quad (10)$$

Any stable weighting function, preferable of low order, can be adopted for W_i^δ, if its magnitude closely bounds the perturbations $|\Delta_i|$ from above.

The feedback controller in each joint should realize accurate tracking of a reference motion, robustly under the considered level of model uncertainty, parasitic effects not covered with the uncertainty model, and disturbances. Mathematically, these objectives can be represented as weighted closed-loop transfer functions that have to be made small through a feedback. Standard transfer functions can be employed (with C_i a feedback controller for the i-th joint):

- Open-loop gain $L_i = P_i C_i$,
- Sensitivity function $S_i = 1/(1 + L_i)$,
- Input sensitivity function $U_i = C_i S_i$,
- Complementary sensitivity function $T_i = 1 - S_i$.

Performance objectives can be specified via frequency dependent weighting functions W_i^S and W_i^U. With W_i^S a desired low-frequency behavior in the closed loop can be enforced, such as a minimum bandwidth requirement and integral control. Attenuation of resonances at low frequencies can be enforced, as well. These are defined by constraining the sensitivity function from above:

$$|S_i(j\omega)| \le 1/|W_i^S(j\omega)|, \ \forall \omega \in \mathbb{R}^+. \quad (11)$$

W_i^U enables enforcing the high-frequency roll-off, which is important for robustness against high-frequency resonances and the measurement noise. Bounding the input sensitivity induces the desired effects:

$$|U_i(j\omega)| \le 1/|W_i^U(j\omega)|, \ \forall \omega \in \mathbb{R}^+. \quad (12)$$

According to the small gain theorem [2], the control of the perturbed plant (5) is robustly stable if the following holds:

$$|T_i(j\omega)| < 1/|W_i^\delta(j\omega)|, \ \forall \omega \in \mathbb{R}^+. \quad (13)$$

Simultaneous specification of above closed-loop control objectives can be done using the block-diagram shown in Fig. 1. In this figure, the channel from q to p is the uncertainty channel with the scalar scaled complex uncertainty δ_i. The channel from w to z_S and z_U should impose the desired performance specifications. If we adopt q and w as the input variables, and p, z_S, and z_U as the output variables, then from Fig. 1 we may determine the interconnecting transfer matrix $\mathbf{H}_i$:

$$\begin{bmatrix} p \\ z_S \\ z_U \end{bmatrix} = \mathbf{H}_i \begin{bmatrix} q \\ w \end{bmatrix}, \ \mathbf{H}_i = \begin{bmatrix} -W_i^\delta T_i & -W_i^\delta T_i \\ W_i^S S_i & W_i^S S_i \\ -W_i^U U_i & -W_i^U U_i \end{bmatrix}. \quad (14)$$

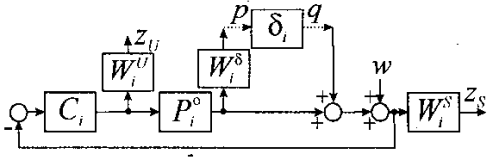

Fig. 1. Set-up for servo design using μ-synthesis

According to μ-analysis theory [2], to have the performance objectives (11) and (12) robustly realized it is sufficient if the structured singular value of the transfer matrix $\mathbf{H}_i$ satisfies

$$\sup_\omega \mu_{\tilde{\Delta}_i}(\mathbf{H}_i) < 1 \quad (15)$$

for the extended plant perturbation structure

$$\tilde{\Delta}_i = \begin{bmatrix} \delta_{SU} & 0 \\ 0_{1\times 2} & \delta_i \end{bmatrix}, \quad (16)$$

where δ_{SU} denotes a complex uncertainty of dimension 1×2. The objective of μ-synthesis is to construct a compensator C_i that stabilizes the feedback loop shown in Fig. 1 and satisfies (15). If such a compensator exists, we say that the robust performance in the given robot joint is realized.

III. Experimental Set-up

The robot shown in Fig. 2, is an experimental facility for the research in motion control [5,8-10]. Its three rotational joints (RRR kinematics) are actuated by gearless brushless DC direct-drive motors. The actuators are Dynaserv DM-series servos with nominal torques of 60, 30, and 15 Nm, respectively. Each actuator has integrated incremental optical encoder having resolution of $\sim 10^{-5}$ rad. The servos are driven by power amplifiers with built in current controllers. The joints have infinite range of motions, since the power and the sensor signals are transferred via sliprings. Both encoders and amplifiers are connected to a PC-based control system. This system consists of the MultiQ I/O board from Quanser Consulting (8×13 bits ADC, 8×12 bits DAC, 8 digital I/O, 6 encoder inputs, and 3 hardware timers), combined with a real-time controller for Matlab/Simulink (Wincon). Such system facilitates control design in Simulink and their real-time implementation. Typically, the controllers run at 1000 Hz sampling frequency. Due to insufficient stiffness in mounting the robot base to the floor, a resonance at 28 Hz is present at the base. There is also a time-delay of two sample times between the control input and the joint angular response [5]. Quantization noise from the incremental encoders is present, as well. These effects are problems often met in practice. Effect of the time-delay can be captured by the modeling part of the procedure presented in this paper. The remaining problems can be tackled by the feedback control design.

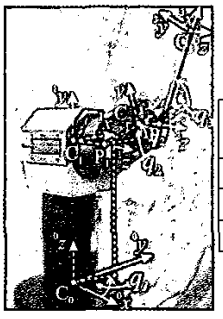

Fig. 2. The RRR robot

TABLE 1. DH PARAMETERS OF THE RRR ROBOT

i	α_i [rad]	a_i [m]	q_i	d_i [m]
1	$\pi/2$	0	q_1	C_0C_1=0.560
2	0	P_1C_2=0.200	q_2	C_1P_1=0.169
3	0	P_2C_3=0.415	q_3	C_2P_2=0.090

Closed-form models of the robot kinematics and dynamics are available in [9]. Their kinematic parameters, according to the well-known DH (Denavits-Hartenberg's) notation [11], are presented in Table 1. The inertial and friction parameters are estimated with sufficient accuracy in [10]. All these allow a real-time implementation of model-based control schemes.

IV. Control Design for the RRR Robot

The kinematic model of the RRR robot computes the reference joint motions given a trajectory of the robot-tip. The dynamic model is used in the control law (2). Stabilisation and desired performance of the robot motions should be realized by feedback controllers designed via μ-synthesis. Here we present the feedback design for the 1st robot joint only. Similar designs are applied to the other joints.

First we explain how the nominal model P_1^o was determined. Fig. 3 presents FRF's measured for $N_1 = 16$ static positions in the joints 2 and 3: $[0\ 0]$, $[0\ \pi/2]$, ..., $[2\pi\ 2\pi]$. These positions span a complete revolution in both joints. It is obvious that the expected behavior of a double integrator, see (3), holds only in the low-frequency region (below 20 Hz), while the real dynamics is much more involved. It is also apparent that up to 4 Hz, the slope of the magnitudes is less steep than –2. This frequency range is within bandwidth of the closed-loop system established via (8). As pointed out in Section II, the spectral components of the measurements within the closed-loop bandwidth are not reliable. However, at low frequencies the dynamics is rigid and is easily determined from the slope of the spectral components beyond the bandwidth. Additional peculiar effects are the resonance around 28 Hz, caused by vibrations at the robot base, and more profound resonances at higher frequencies. It is also clear that at low frequencies the phase does not remain at $-180°$, but has a lag growing with increasing frequency. The phase lag is the consequence of the time-delay. The nominal FRF $G_1^o(j\omega)$, calculated with (9b), is presented in Fig. 3 by the bold line. It is repeated in Fig. 4, together with Bode plots of the parametric fit $P_1^o(j\omega)$ determined using the output error model structure with a least-square criterion [7]. The discrepancy between the unreliable data below 4 Hz and the fit is obvious. In addition to determining P_1^o, FRF's corresponding to the cross-couplings between joint 1 and the remaining joints were measured. At each frequency within the range of rigid dynamics, the amplitude of $P_1^o(j\omega)$ was at least two orders of magnitude higher than the amplitude of any of the cross couplings. This justifies independent feedback control design for each joint of the RRR robot.

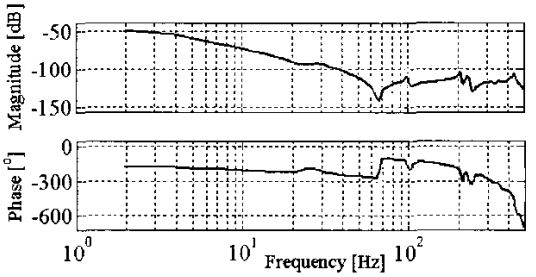

Fig. 3. Experimental FRF's $G_1^1,\ldots,G_1^{16}$ (thin) and the nominal FRF G_1^o (bolded)

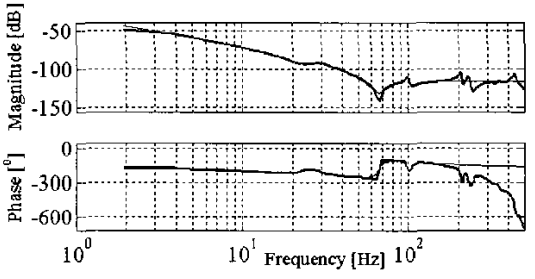

Fig. 4. Bode plots of the nominal data G_1^o (thick) and of the parametric fit P_1^o (thin)

The thin lines in Fig. 5 present relative differences in mag-

nitude between each $G_1^1,\ldots,G_1^{16}$ and P_1^o. By virtue of (10), at each ω the maximum perturbation from the nominal plant model is represented by Δ_1. It is shown in Fig. 5 with the bold line. The dotted line in the same figure represents the magnitude of the parametric weighting function W_1^δ, in accordance with (7). As already noted, the FRF's of the measured data below 4 Hz are inaccurate, and hence W_1^δ does not bound the uncertainty in the lower frequency range. Fig. 6 shows the performance weightings W_1^S and W_1^U. The former one is chosen such that integral control is achieved, together with as high as possible reduction of the position error at low frequencies. Furthermore, it should enforce attenuation of the vibrations at 28 Hz. The latter one should enforce the high-frequency roll-off.

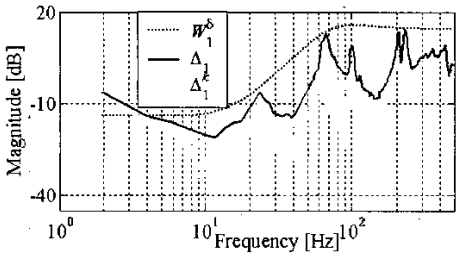

Fig. 5. Magnitude plots of the weighting function W_1^δ, of relative differences between P_1^o and $G_1^1,\ldots,G_1^{16}$, and envelope of all differences Δ_1

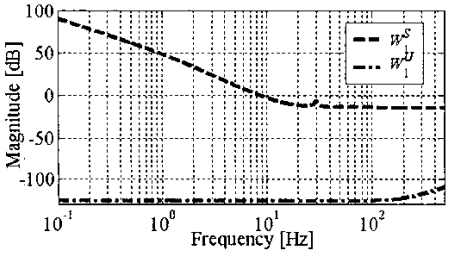

Fig. 6. Magnitude plots of the performance weighting functions W_1^S and W_1^U

Finally, a feedback controller was designed using μ-synthesis that employs iterative scaling of the 2nd order (D-scaling [2]) and H_∞ optimization. Five DK iterations were necessary to determine C_1 ensuring robust performance specified by W_1^S and W_1^U in Fig. 6, for the range of uncertainty given in Fig. 5. The Bode plots of the resulting C_1 are shown in Fig. 7. The controller introduces integral action at low frequencies, and deals with various resonance frequencies over a broad frequency range. A plot of the upper bound of the achieved structured singular value $\mu_{\mathbf{H}_i}$ is given in Fig. 8. It is below 1, which implies a satisfactory design.

V. Assessment of the Control Design

Let us first verify that the feedback controller designed in the previous section guarantees robust stability and robust performance. Fig. 9 shows magnitude plots of the complementary sensitivity functions of the closed-loop system with the compensator C_1, calculated for the nominal plant model P_1^o and for all $G_1^1,\ldots,G_1^{16}$. Since all the plots satisfy the condition (13), it is confirmed that the system remains stable for all postures.

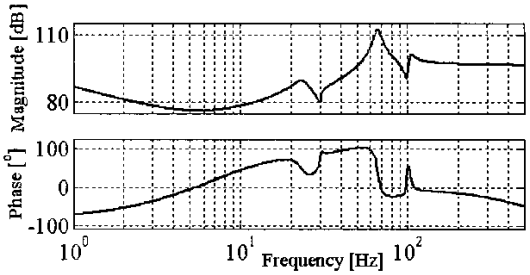

Fig. 7. Bode plots of the feedback controller C_1

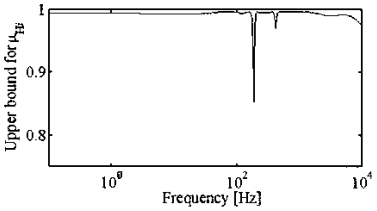

Fig. 8. Upper bound of the structured singular value for the 1st joint

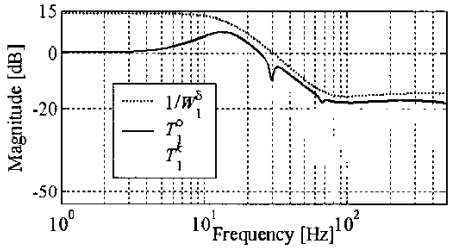

Fig. 9. Magnitude plots of the nominal and of the perturbed complementary sensitivity functions are below $|1/W_1^\delta|$

In Fig. 10 we show plots of the sensitivity functions (top) and of the input sensitivity functions (bottom), calculated for all 16 positions and for the nominal model. As all the plots are bounded with the magnitudes of $1/W_1^S$, respectively, $1/W_1^U$, we conclude that the performance specifications are robustly satisfied, i.e., the conditions (11) and (12) are satisfied for all postures. Results similar to those presented in Figs. 8-10 also hold for the other two joints of the RRR robot.

To experimentally verify robust performance of the robot, the reference motion task given in Fig. 11 was considered. It required all the joints to be displaced for π radians in 1 [s], with zero initial/terminal speed and acceleration. Such motion required the full authority of the drives, and it was experimentally realized using the designed controllers.

The achieved position errors are shown in Fig. 12 with black lines. For comparison, the errors obtained with the

best-tuned conventional PD feedback controllers [5] are depicted in the same figure with gray lines. With the robust feedback, the errors in joints 1 and 2 remained within the range $[-10^{-3},10^{-3}]$ radians, with PD they were within $[-2.5\cdot10^{-3}, 2.7\cdot10^{-3}]$, respectively, $[-1.7\cdot10^{-3}, 2.8\cdot10^{-3}]$ radians. In joint 3, the robust feedback achieved an error twice that of the first two joints, while the PD achieved the range $[-4.1\cdot10^{-3}, 7\cdot10^{-3}]$ radians. Obviously, the robust feedbacks realized the reference motions more accurately. The obtained accuracy is very good for a direct-drive robot. To evaluate if the reduction of the tracking error was below the prescribed one, we found the ratio between the spectra (determined by Fast Fourier transform) of the error e_1 and of the reference $q_{r,1}$. The ratio is plotted in Fig. 13, together with inverse of the weighting function W_1^S. Apparently, the curve corresponding to the ratio is always below the weighting. Having in mind the relation $S_1 = e_1 / q_{r,1}$, it follows that condition (11) was satisfied, i.e., the specified error reduction was realized. It appears that robust performance control of the RRR robot was realized in the experiment.

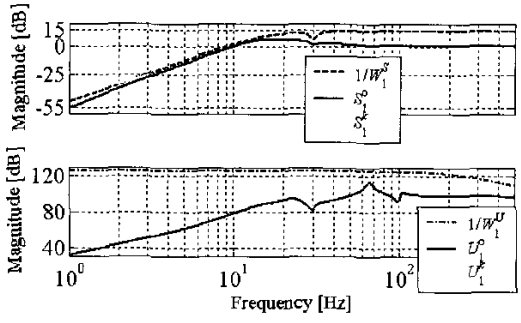

Fig. 10. Magnitude plots of the nominal and of the perturbed sensitivity functions (top), and of the nominal and of the perturbed input sensitivity functions (bottom)

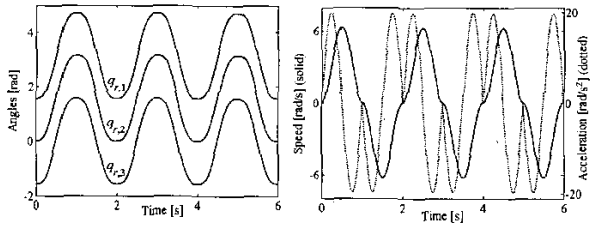

Fig. 11. Experimental reference motion task

Finally, we point out that the suggested procedure does not provide the best accuracy in realizing the reference motions. In [5] we present position errors for the motion task defined in Fig. 11, obtained with feedback designed via loop-shaping and H_∞ optimization. These errors are 10-20 % lower than the errors shown in Fig. 12, but the feedback design from [5] does not ensure robust performance. As robust performance is a desirable property in practice, we believe that further research should be focused on feedback control design techniques ensuring such a property, but with increased performance. A factor influencing the level of performance is the representation of model uncertainty. We expect that representing the uncertainty using a linear parametrically varying (LPV) model and designing the appropriate LPV controller, may achieve a performance improvement.

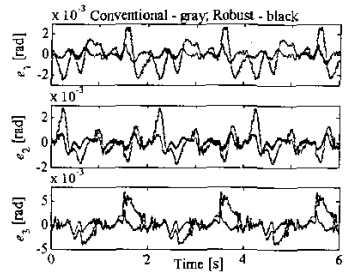

Fig. 12. Experimental position errors

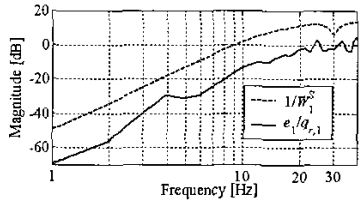

Fig. 13. Ratio between spectra of the position error (robust feedback) and of the position reference is below $1/W_1^S$

VI. Conclusion

This paper presents a procedure to realize robust control performance of a robot. It computes the controllers in a systematic way, taking into account experimental characteristics of the robot. Uncertainty of the known dynamic model is characterized from several frequency responses measured directly. The desired performance is specified in the frequency domain. Uncertainty models and performance specifications are used in a μ-synthesis design of joint servo controllers. The procedure is validated on a direct-drive robot. Experimental results indicate that robust performance is realized.

References

[1] H.G. Sage, M.F. de Mathelin, E. Ostertag, "Robust Control of Robot Manipulators: A Survey," *Int. J. Control*, Vol. 72, No. 16, pp. 1498-1522, November 1999.

[2] K. Zhou, J.C. Doyle, K. Glover, *Robust and Optimal Control*, Prentice Hall, Upper Saddle River, 1996.

[3] G.J. Balas, J.C. Doyle, K. Glover, A. Packard, R. Smith, *μ-Analysis and Synthesis Toolbox*, The MathWorks Inc., Natick, MA, 1998.

[4] J.J.E. Slotine, W. Li, *Applied Nonlinear Control*, Prentice Hall, London, 1991.

[5] D. Kostić, B. de Jager, M. Steinbuch, "Experimentally Supported Control Design for a Direct Drive Robot," *Proc. IEEE Int. Conf. Control Appl.*, pp. 186-191, Glasgow, Scotland, September 2002.

[6] M. Vukobratović, V. Potkonjak, *Dynamics of Manipulation Robots: Theory and Application*, Springer-Verlag, Berlin, 1982.

[7] C.K. Sanathanan, J. Koerner, "Transfer Function Synthesis as a Ratio of Two Complex Polynomials," *IEEE Trans. Autom. Control*, Vol. 8, No. 1, pp. 56-58, January 1963.

[8] B. van Beek, B. de Jager, "RRR-Robot Design: Basic Outlines, Servo Sizing, and Control," *Proc. IEEE Int. Conf. Control Appl.*, pp. 36-41, Hartford, CT, October 1997.

[9] D. Kostić, R. Hensen, B. de Jager, M. Steinbuch, "Closed-form Kinematic and Dynamic Models of an Industrial-like RRR Robot," *IEEE Conf. Rob. Autom.* pp. 1309-1314, Washington D.C., May 2002.

[10] D. Kostić, R. Hensen, B. de Jager, M. Steinbuch, "Modeling and Identification of an RRR-robot," *IEEE Conf. Dec. Control*, pp. 1144-1149, Orlando, FL, December 2001.

[11] L. Sciavicco, B. Siciliano, *Modeling and Control of Robot Manipulators*, McGraw-Hill, London, 1996.